IEEE Access
Multidisciplinary | Rapid Review | Open Access Journal

Received January 9, 2020, accepted January 21, 2020, date of publication February 17, 2020, date of current version March 3, 2020.

Digital Object Identifier 10.1109/ACCESS.2020.2974262

Detection of Apple Defects Based on the FCM-NPGA and a Multivariate Image Analysis

WENZHUO ZHANG, JUAN HU, GUOXIONG ZHOU, AND MINGFANG HE

College of Computer and Information Engineering, Central South University of Forestry and Technology, Changsha 410004, China

Corresponding author: Guoxiong Zhou (51840157@qq.com)

This work was supported by the National Natural Science Foundation of China under Grant 6170344.

(*Wenzhuo Zhang and Juan Hu contributed equally to this work.*)

ABSTRACT In existing machine vision technology for fruit defects, the hue appears different, and the defect area is small due to the irregularity of illumination reflection from the surface incident light source, this makes it difficult to extract the defect area. Thus, we proposed an apple defect detection method based on the Fuzzy C-means Algorithm and the Nonlinear Programming Genetic Algorithm (FCM-NPGA) in combination with a multivariate image analysis. First, the image was denoised and enhanced through fractional differentiation. The noise points and edge points were removed, and the important texture information was preserved. Then, the FCM-NPGA algorithm was used to segment the suspicious defect graph. Finally, a method based on a multivariate image analysis strategy was used to detect the flaws of the apple's suspicious defect map. The application results of 2000 images showed that the overall detection accuracy was 98%. Experiments show that the apple defect detection algorithm based on FCM and NPGA combined with multi-image analysis method is effective.

INDEX TERMS Apple defect detection, fractional calculus, multivariate image analysis, FCM, NPGA.

I. INTRODUCTION

At present, the technology after fruit picking for surface defect detection, grading, and sorting is relatively backward in China, resulting in the low cost of fruit processing, inferior fruit quality, poor sales, and low economic benefits [1]. The economic benefits of fruit processing in China can be significantly increased by the automatic detection technology of fruit surface defects. This means that real-time computer vision technology is objective and non-destructive, making it suitable for the identification and rapid detection of surface defects in agricultural products such as apples.

Using monochromatic imaging with a band-pass or long-pass filter to detect apple defects has been reported in early studies. Defects were detected by applying simple thresholding to acquire gray-scale images and computing shape features such as circularity of segmented components [2]. However, simple thresholding usually cannot yield satisfactory segmentation because the curvature of the fruit would cause the intensity of images to be distorted; the gray level of these images normally decreases from the center to the edge, with large variations in the size, shape, and texture of defects. In this case, a spherical grayscale transformation method was proposed by literature [3]. Defects on the fruit surface could be segmented using a single threshold, which solved the problem that the gray value of the defective part in the middle of the fruit image is higher than that of the normal part on the edge; however, it could not be segmented successfully at one time. Besides, multi-thresholding and adaptive thresholding techniques can also be used to improve defect segmentation; unfortunately, they take intensive computation time [4]. An alternative to thresholding is region-based segmentation, which finds coherent, homogeneous regions based on a similarity criterion. Particularly, in literature [5] proposed a region-based flooding algorithm to detect patch-like defects such as bruises on apples by treating apple images as geographic landscapes and the patch-like defects as catchment basins in the landscapes. Then, it was further improved by using active contour models to closely surround the defects. However, such methods cost more computation time than thresholding techniques.

With the development of multispectral, hyperspectral imaging, and other emerging optical modes, traditional monochrome imaging technology has gradually been

The associate editor coordinating the review of this manuscript and approving it for publication was Mustafa Servet Kiran.

replaced by hyperspectral technology in the field of apple defect detection [6]. For example, the application of hyperspectral imaging technology to detect internal damage in a kiwifruit peel was presented by literature [7]. In their study, visible near-infrared images with spectral wavelengths ranging from 408 to 1117 nm were used to collect hyperspectral image data. Besides, a principal component analysis (PCA) was employed to extract effective bands. The experimental results demonstrated that the detection rate of damage was 85.5%. Moreover, through a PCA and a support vector machine (SVM) to construct a classification model of the degree of apple damage, literature [8] investigated the optical properties of apples damaged in different degrees in the wavelength range of 400 $\sim$ 1050 nm. The classification accuracy reached 92.5%. However, this method relied on sampling apple slices for detection, causing the integrity of the apples to be destroyed. Literature [9] developed a non-destructive method using X-ray CT images. The gray level thresholds of ''Jonagold,'' ''Joly Red,'' and ''Kanzi'' apples were calculated by the multi-level Otsu threshold method. The damage volume in the apple's equatorial region was automatically detected and quantified by the method. However, this method not only comes with a long detection period but it also emits radiation. Furthermore, the technology is extremely strict in security requirements and is not suitable for wide application. Literature [10] studied Jonagold apples that had been damaged within the last two hours. They applied the particle filter algorithm to the post-processing image and built a pixel-based PLS-DA model by improving the spectral signal-to-noise ratio. The recognition rate of apple damage was 96%. Moreover, literature [11] applied active infrared thermal imaging technology based on the hypothesis that internal damage and physiological imbalance of an apple led to changes in tissue thermal properties. They succeeded in identifying early damage at different depths in thermal image sequences. Unfortunately, the image resolution and contrast were low. Then, literature [12] presented a novel automatic defective apple detection method combining computer vision system with automatic lightness correction, number of defect candidates (including true defects, stem defects, and calyx defects), region counting, and weighted relevance vector machine (RVM) classifier. The experimental results illustrated that the overall detection accuracy of 160 samples was 95.63%. Besides, browning inside a Fragrant pear was detected using magnetic resonance imaging (MRI) in the study of literature [13]. Image processing was applied to separate the nucleus from the browned part in their study; the misjudged browning slice images were further analyzed. The final recognition rate was 100%. However, nuclear magnetic resonance technology has a problem of high equipment costs.

In the field of machine vision, whether the apple is damaged is determined mainly through the photograph of the apple skin defect photograph. Literature [14] detected the disease of green apples using back propagation (BP) neural network based on genetic algorithm (GA) and SVM optimization. The experimental results can reach an accuracy of 92.1%. Although good results were obtained, the process was too complicated and took a lot of time. In the research of literature [15], the image of the apple region was obtained through morphological operations and hole filling; then, median filtering and edge detection algorithms were used to extract the shape, color, and defect features of the apple; finally, the particle swarm optimization SVM was applied to classify apples, reaching the accuracy of 92%. Literature [16] first extracted the texture features of apples such as discrete wavelet feature, the histogram of oriented gradients (HOG), Law's Texture Energy (LTE), Gray level co-occurrence matrix (GLCM), and Tamura features. Then, SVM was used to classify apples. However, the detected defect area is generally not accurate enough because of the application of image smoothing technology in the algorithm. The basis of fruit visual recognition and location is the selection of image segmentation technology, which can segment fruits from a complex background quickly, accurately, and without omission. Particularly, literature [17] first employed Oust algorithm to segment the apple defect image to determine the defect area; then, Canny edge detection algorithm and particle swarm algorithm with a lag threshold was used to detect the defect area in order to obtain apple defect features; finally, the features were inputted. Recognizing the SVM model, the experimental accuracy of 91% can be obtained. Besides, the K-means clustering segmentation algorithm combined with the convex hull theory was used by literature [18] to segment and reconstruct overlapping target fruits. Similarly, literature [19] proposed an improved Otsu maximum inter-class variance method for image segmentation based on the R-G color difference model. The accumulator, search range, and center distance were set according to the side length of the minimum circumscribed rectangle of the apple. The experimental results illustrated that the correct recognition rate was 84.7%. Based on a multi-scale visual significance improvement, literature [20] proposed a fuzzy clustering algorithm for fruit image segmentation. In their study, 50 images of 100 mature lychees and other citrus fruits were randomly selected to perform the image segmentation experiment. The results demonstrated that the average fruit segmentation rates of the mature lychees and citrus fruits were 95.56% and 93.68%, respectively. Moreover, literature [21] proposed a fruit image segmentation algorithm based on the ant colony algorithm. Although the accuracy of the algorithm was verified, whether the algorithm could meet the requirements of a mobile terminal within a specific segmentation time was not analyzed. Subsequently, literature [22] proposed an improved fuzzy clustering image segmentation method depending on artificial bee swarm optimization; this method involved optimization based on a traditional artificial bee colony. The fruit image was segmented according to the principle of a maximum membership degree. The improved image segmentation method could be used to segment fruit from the natural environment. The average segmentation time of a single image was 0.2193s; the correct segmentation rate was 90.33%. The above research

results revealed that the key to the detection of fruit surface defects and the automatic classification of the fruit was to accurately segment the defective parts from the image of the fruit surface. Therefore, our predecessors have performed various meaningful discussions and proposed many defect segmentation and detection methods.

The key problem of apple surface defect identification lies in whether it can effectively be used to identify the presence, size, location, and other characteristics of apple surface defects. The extraction of those features generally relies on manual separation, which comes with high labor intensity, low productivity, and unstable sorting accuracy. As a method of image analysis [23], multivariate image analysis has been widely used in satellite imaging, medical imaging, and micro image processing [24]. However, it is usually difficult to guarantee the accuracy of apple surface defect detection when solving specific problems in a certain field directly using multivariate statistical analysis (such as the apple surface defect detection discussed in this paper).

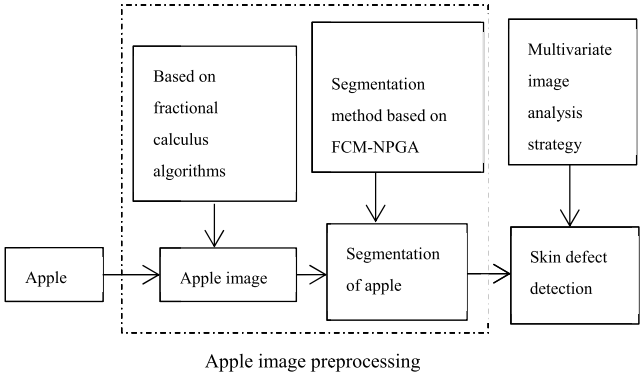

FIGURE 1. The schematic diagram of system operation.

In order to solve the above problems, we proposed a fruit surface defect detection method based on FCM-NPGA and a multiple image analysis strategy. The working principles of the method are shown in Fig. 1. First, collected apple images had to be preprocessed. Image preprocessing covered denoising enhancements and segmentation. The image denoising enhancement algorithm based on a fractional calculus was used to remove the noise and edge points to retain important texture information. In the segmentation process, the segmentation method based on FCM-NPGA was adopted to achieve the successful segmentation of fruit skin with defects in complex patterns. The application results indicated that the FCM-NPGA method more accurately separated and segmented the defects of the apple than did the traditional FCM segmentation algorithm, which allowed us to mark the defects of the apple.

The rest of the paper is organized as follows. Section 2 introduces methods of this paper. Section 3 gives the analysis of experimental results. We make a conclusion in Section4.

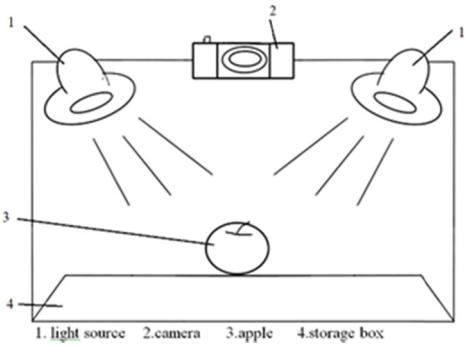

FIGURE 2. Image acquisition device.

II. FRUIT DEFECT DETECTION

A. DATA ACQUISITION

Image acquisition is a vital part of a defect detection system. The quality of fruit detection and sorting is determined directly by the quality of the image information acquisition. The apples used as samples in this study were purchased from a local fruit wholesale market in Changsha in August 2018. Their variety is known as Yantai, originating from the Shandong Province. The image acquisition device consisted of a Canon 5D3 digital camera and a closed lighting system, as shown in Fig. 2. We collected images of apple scratches, cracks, crushed parts, rotted parts, and other common defective and intact images. The size of the picture was 2880×1920 px, and the format was jpeg. Although the highest pixel of the camera is 5760×3840, but because of the calculation needs, this article sets the pixel of the picture to 2880×1920.

The data set used in this study included 2000 apple pictures, of which 1200 were intact apple pictures included in the training sample set, and 800 were defective apple pictures included in the test sample set. The verification set was Ground Truth with a total of 800 samples. The camera equipment we adopted was the Canon 5D3, with the highest resolution being 5760×3840 px, and the storage medium being an SD card. This machine was equipped with Intel i7-cpu, 12 GB of memory. We also used a LENOVO XIAOXIN310 laptop. The algorithm software environment was opencv $3.4 + \mathrm{VS2017} + \mathrm{C}++$.

To generate high-resolution images, two key conditions had to be met. First, the range of light source had to be concentrated in the range of camera shooting, the light had to be irradiated in the frontal field, and the light had to be even to avoid the generation of shadows and specular reflections. The second requirement was to reflect most of the light from the apple back into the camera. During image acquisition, the light source was placed directly in front of the apple, and the apple was placed in the camera shooting range to take a complete optical image of the apple. Subsequently, the obtained optical image was converted into a digital image. We used the image acquisition card to transmit the acquired image information to the computer, and then waited for the next apple image to process. Some of the apple images collected are shown in Fig. 3.

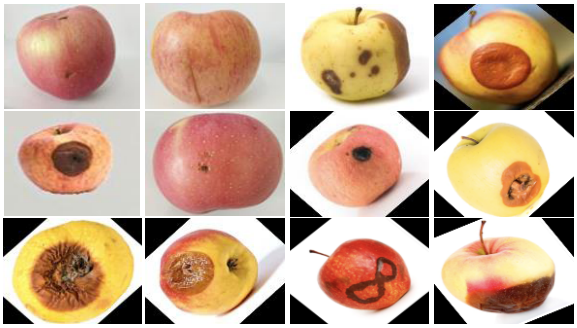

FIGURE 3. Collected apple images.

B. APPLE IMAGE PREPROCESSING

1) APPLE IMAGE DENOISING ENHANCEMENT BASED ON A FRACTIONAL CALCULUS ALGORITHM

In image analysis, input images often have several disadvantages (e.g., noise and insufficient contrast) due to different image environments for image acquisition (e.g., the brightness of light and the quality of equipment performance). Moreover, distance and focal length make the size and position of fruit in the middle of the whole image uncertain. To ensure the consistency of fruit size, position, and quality in the fruit image, the image must be preprocessed. The major aim of image enhancement and de-noising in our study was to eliminate irrelevant information in the image, remove interference and noise, recover useful information, enhance the detectability of relevant information, and minimize data to improve the reliability of feature extraction. The fractional calculus algorithm showed high accuracy and effectiveness in image processing. This algorithm could not only remove noise, but also enhance the edge detail texture information of the image. The image with noise was de-noised and enhanced synchronously.

a: DEFINITION OF FRACTIONAL CALCULUS [25]

When y was equal to $f(t)$ for a function with the independent variable of t and the independent variable value range of (a, b), the fractional calculus of order v of the function $f(t)$ was written as follows:

$$ {}_aD_b^v f(t) D^v f(t) \tag{1} $$

In Equation (1), a and b denote the range of values of the independent variable t, $f(t)$ denotes a signal; $f(t) \in (a, t)$ $(a < t, a \in R, t \in R)$, v denotes a differential order; D denotes a differential or integral.

Equation (1) represents the order of calculus as a fraction. When the fractional derivative of order v was a fractional derivative, It was termed as a fractional integral if $v < 0$. Thus, there has been no uniform time-domain expression for fractional calculus [26].

Due to the separability of the two-dimensional Fourier transform, the backward difference of fractional derivatives in the negative x direction and negative y direction could be expressed as follows [27]:

$$ \begin{cases} \dfrac{\partial^v f(x,y)}{\partial x^v} \approx f(x,y) + (-v) f(x-1,y) \\ \quad + \dfrac{(-v)(-v+1)}{2!} f(x-2,y) \\ \quad + \ldots + \dfrac{\Gamma(-v+n)}{\Gamma(n+1)\Gamma(-v)} f(x-n-1,y) \\ \dfrac{\partial^v f(x,y)}{\partial y^v} \approx f(x,y) + (-v) f(x,y-1) \\ \quad + \dfrac{(-v)(-v+1)}{2!} f(x,y-2) \\ \quad + \ldots + \dfrac{\Gamma(-v+n)}{\Gamma(n+1)\Gamma(-v)} f(x,y-n-1) \end{cases} \tag{2} $$

It is common to calculate the whole image using a pixel mask with operators when fractional order differentiation is employed to process images. The first n term coefficients of the difference Equation were yielded through Equation (2), the coefficients were uniformly expressed as a function of order v as follows:

$$ \phi_\varepsilon(k) = \frac{\Gamma(-v+1)}{k!\Gamma(-v+k-1)} \tag{3} $$

where v denotes the fractional differential order. Coefficients representing different positions in the template were $k = 1 \ldots n$. In this study, the fractional order differential mask operation was performed on the image from eight directions. The coefficients in each direction template were denoted as $\phi_{0^\circ}(k)$, $\phi_{45^\circ}(k)$, $\phi_{90^\circ}(k)$, $\phi_{135^\circ}(k)$, $\phi_{180^\circ}(k)$, $\phi_{225^\circ}(k)$, $\phi_{270^\circ}(k)$, and $\phi_{315^\circ}(k)$.

b: IMAGE ENHANCEMENT REGION DEFINITION

In this paper, the local statistical features of the image [28] (local mean and local standard check) are introduced to perform differential and selective enhancement of the image in order to improve the efficiency and accuracy of the algorithm.

In the two-dimensional image, Q denotes the pixel point with the coordinates of (i, j); $f(i, j)$ is the gray value of pixel point Q; W_{xy} is a $N \times N$ square filtering template centered on Q. In accordance with the knowledge of probability theory, the local mean was defined as follows:

$$ E_p = \frac{1}{N^2} \sum_{i=1}^{N} \sum_{j=1}^{N} f(i,j). \tag{4} $$

The local variance (local contrast) of the image was expressed as:

$$ \sigma_p^2 = \frac{1}{N^2} \sum_{i=1}^{N} \sum_{j=1}^{N} (x(i,j) - E_p)^2 \tag{5} $$

c: IMAGE DENOISING ENHANCEMENT ALGORITHM BASED ON FRACTIONAL CALCULUS

First, the local mean and the local standard deviation were compared with the global statistical information to define the regions that had to be enhanced from those that did not need to be enhanced. Also, the regions that had to be enhanced were processed using fractional differential masks.

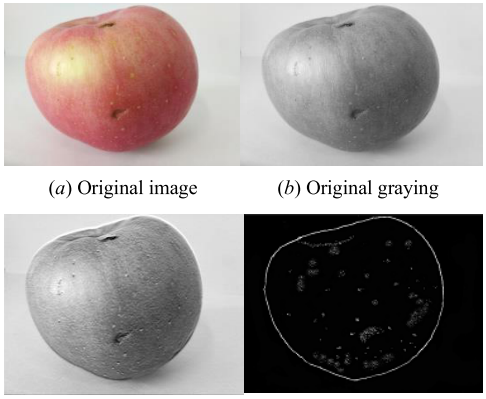

(*a*) Original image (*b*) Original graying

(*c*) Enhanced denoising result map (*d*) Image edge detection

FIGURE 4. Enhanced de-noising intent.

Since the differential order was built according to the local gradient modulus and entropy of the image, the differential order could be adaptive. Subsequently, the image denoising enhancement algorithm based on fractional calculus was employed to detect the suspicious noise points and judge the edge of the noise. The noise points were denoised through fractional integration, and the edge points were enhanced through fractional differentiation. Non-noise points and non-edge points retained their original values, allowing us to obtain important texture information. The apple image below was selected from the data set using Visual Studio 2017. The original image was processed through a gray image and then simulated; the process of enhancement and denoising is illustrated in Fig. 4.

Fig. 4 (a) is the original defect image of the apple, Fig. 4 (b) is the apple's original defect image without adding other noise (grayed), Fig. 4 (c) depicts the denoising enhancement algorithm based on fractional calculus for denoising and enhancement of noisy images, and Fig. 4 (d) depicts the edge detection after enhanced processing.

Fig. 4 shows that the algorithm simultaneously denoised and enhanced the apple defect image that was used. Since the apple image in the data set was clear, edge detection was used to verify the processing to more clearly observe the effect of enhanced denoising, as shown in Fig. 4 (c). After the denoising enhancement, the edge of the image was prominent, and the detail information was intact, which contributed to the accurate location of the defect segmentation in the next step.

Peak signal-to-noise ratio (PSNR) [29] is a significant indicator for measuring image quality. In this paper, the image quality is measured by comparing the PSNR of the images. The structures of the noise reduction image and the original image are compared by calculating the structural similarity index measurement (SSIM) [30] between them. The value range of SSIM is [0, 1]. The larger the value, the better the image quality.

As can be seen from Table 1, the image denoising algorithm based on fractional difference has higher PSNR and SSIM compared to wavelet denoising [31] and mean filtering

TABLE 1. Enhanced denoising comparison results.

	PSNR	SSIM
Wavelet denoising	19.178	0.839
Mean filter denoising	24.256	0.947
Fractional differential denoising	34.451	0.979

denoising [32]. It can be found by analyzing the data in the table that the denoising and edge-preserving capabilities based on the fractional difference algorithm are generally superior to those on the wavelet denoising and mean filter denoising.

2) A SEGMENTATION METHOD BASED ON FCM-NPGA

After denoising and enhancing the apple's original image based on the fractional calculus algorithm, the following segmentation boundary turned out to be clearer, and whether the surface defect region could be accurately segmented from the image was verified; this was the key of the main operation and success of the whole defect detection process.

The FCM algorithm [33] is an efficient method for apple surface defect segmentation. However, only the fuzzy mean algorithm is applied for apple image segmentation. The result is easily affected by noise and instability. Accordingly, the use of the fuzzy mean algorithm combined with the non-linear programming GA not only made the local details more abundant, but also ensured the global optimum. Thus, the apple image segmentation effect was more obvious.

a: FCM ALGORITHM

We assumed there was a set of original image data I of $n * n = N$, and the n data points were mapped to a one-dimensional space according to (6). We set the N data samples as $X = \{x_1, x_2, \ldots, x_N\}$.

$$arr_2[i][j] = arr_1\left[\frac{(i-1)*n - i*(i-1)}{2+j-i}\right]. \quad (6)$$

In Equation (6), i, j represents the coordinates mapped to the one-dimensional space, and n represents the pixel dimension of the original picture.

When classifying things, given a value c, the data was stratified into $c\,(2/c/N)$ types, and $(A_1, A_2, \ldots, A_N)$ was used to represent c specific divisions. U denoted a similar classification matrix, using $\{v_1, v_2, \ldots, v_c\}$. For a given partition, μ_{ik} was the membership of the sample (x_i) to the A_k like cluster. Criterion J_b was divided as follows:

$$J_b(U, v) = \sum_{i=1}^{N}\sum_{k=1}^{c}(u_{ik}^b)(d_{ik})^2 \quad (7)$$

where $d_{ik} = \sqrt{\sum_{j=1}^{m}(x_{ij} - v_{kj})^2}$, and d_{ik} is the Euclidean distance, which measures the distance between the i sample x_i

and the center point of the k class. In this method, an optimal partition was obtained. In image segmentation, the segmentation region was obtained, and the objective function J_b reached the minimum value.

b: NPGA

Though the GA is an algorithm based on global optimization, it often ignores the local optimal solution [34], [35], thereby omitting some details. Thus, the idea of nonlinear programming was introduced [36], [37]. In the FCM clustering algorithm, when the nonlinear programming was introduced to the image segmentation theory, the constraint condition of the unknown variables was that the sum of the membership values of the samples for each given class was equal to 1, expressed as follows:

$$\sum_{j=1}^{c} \mu_j(x_i) = 1 \quad i = 1, 2, \ldots, N \tag{8}$$

In this algorithm, to minimize (7), the necessary conditions indicated in the following Equation had to be satisfied as well:

$$\begin{cases} u_{ik} = \dfrac{1}{\sum_{j=1}^{c} \left(\frac{d_{ik}}{d_{lk}}\right)^{\frac{2}{b-1}}} \\ v_{ij} = \dfrac{\sum_{k=1}^{N} u_{ik}^{b} x_{kj}}{\sum_{k=1}^{N} u_{ik}^{b}} \end{cases}. \tag{9}$$

The two expressions in (9) were used to calculate the membership degree (u_{ik}) and the c clustering centers $\{v_i\}$ of sample x_i for class A_k, respectively. The FCM clustering algorithm employed (9), repeatedly modifying the clustering center and classifying the data membership degree when the algorithm converged. From the above calculations, each partition center could be obtained. From the perspective of image processing, each point to the corresponding division of the degree of attribution could also be calculated. Thus, the fuzzy division was completed, and the image segmentation was also carried out simultaneously.

Usually, researchers use the concept of gradient descent to solve the final constraint problem of nonlinear programming. although we could have obtained the so-called local optimal solution at a certain interval, the search ability of the whole situation is very weak. in contrast, the ga, using selection, crossover, and mutation operators, could maximize the diversity of individuals and maximize the global search ability of the algorithm. however, the local search ability of this method is weak, and it is particularly sensitive to the initial value of the clustering center, so it can only get the sub-solution of the target, not the optimal solution. therefore, in this study, we combined the advantages of the two algorithms and set an integer, n. when the evolutionary algebra was a multiple of the integer n, we carried out the related operation of nonlinear programming; otherwise, the related steps of the ga were performed in the loop. the application of the npga not only improved the local search ability, but it also ensured the global optimal solution of the algorithm, as allowing to get a better segmented image.

c: APPLE SURFACE DEFECT SEGMENTATION BASED ON FCM-NPGA

After enhancing and denoising the apple image by fractional calculus, the geometric feature image data were generated. On that basis, the image segmentation technology based on FCM-NPGA was used for the image segmentation. In the core step of image segmentation, the design of a coding scheme in the gene and fitness function in the GA had to be considered in the segmentation algorithm (FCM-NPGA) based on FCM and NPGA algorithms.

The coding scheme used in this study was as follows: Divide n data into c-type, and use gene string $a = [T_1, \ldots, T_i, \ldots, T_n]$ to represent a class of results, where the value of T_i is $1, 2, \ldots, c\,(i = 1, 2, \ldots, n)$. When the value of T_i was equal to $k\,(1 \leq k \leq c)$, the ith data belonged to the k-class. The search space of this scheme had c^n points, and we used (9) as the fitness function of the GA to carry out the relevant operation of the GA. We set N as the current evolutionary algebra and n as the set number of evolutions. For image segmentation based on the FCM and NPGA algorithms, the specific steps were as follows:

A. Apple Image Segmentation based on FCM-NPGA:
   a. Population initialization;
   b. Fitness function calculation;
   c. Selective crossover and variation;
   d. Regeneration population;
   e. If the number of evolutions, N, could be divided by n, go to step (g); otherwise, go to step (f);
   f. Non-linear programming processing;
   g. If the number of evolutions reached the set n, go to step 2; otherwise, go to step (b);
B. Decoding and applying the optimal partition to the preprocessed apple image; Outputs the split result.

The process is shown in Fig. 5.

This paper uses the Davies-Bouldin Index (DBI) [38] indicator to determine the number of categories of clusters. Fig. 6 shows the corresponding DBI indicator when the number of categories of clusters is 3-10. It can be seen that when the number of clusters is 3, the DBI indicator is the lowest. We set the number of cluster centers to three. Fig. 7 (a) shows an enhanced denoising image of an apple. Fig. 7 (b) is the result of clustering. The imaging depicted in Fig. 7 (c) can be used for segmentation and to obtain general hierarchical information.

After denoising and edge enhancement of the apple image, the noise and some blurred regions in the image improved. Subsequently, the algorithm was employed to maximize the result of defect segmentation and determine the suspicious defect blocks, thereby facilitating the next step of defect detection processing, avoiding global scanning detection, and reducing the number of tasks, and improving the accuracy.

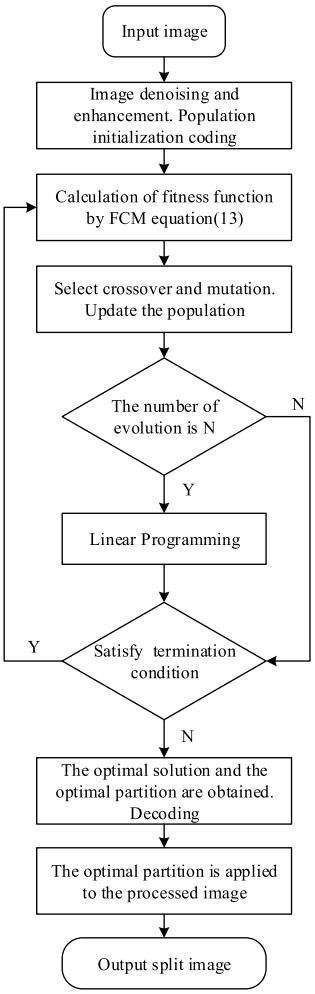

FIGURE 5. Flow chart of FCM-NPGA algorithm.

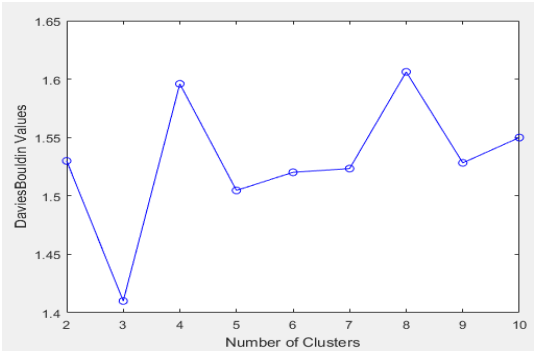

FIGURE 6. Number of clusters of DBI indicators.

C. APPLE DEFECT DETECTION BASED ON MULTIVARIATE IMAGE ANALYSIS

After segmentation, suspicious defects are identified, yet they often cannot be identified as defects. This is because the extraction of apple surface defects requires high uniformity in the light source; uneven illumination often causes false detection and missed detection of defects [39].

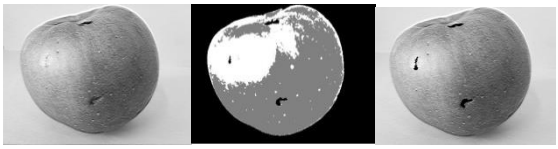

FIGURE 7. Image segmentation for the FCM-NPGA. (a) shows an enhanced denoising image of an apple. (b) is the result of clustering. The imaging depicted in (c) can be used for segmentation and to obtain general hierarchical information.

Multivariate image analysis refers to an image analysis method based on multivariate statistical analysis [40], [41]. The variable number of multi-variable images can be reduced by using an intact apple image and apple surface defect image to construct a multi-variable image and analyzing and optimizing the choice of variable number. Moreover, the requirement of uniformity in the light source is low. The accuracy and reliability of defect detection are generally improved as a result.

1) MULTIVARIATE APPLE IMAGE PROCESSING BASED ON A PCA

A J-row, I-column image matrix consisted of a gray-scale image of the size of $I \times J$ pixels. The registered M different images were stacked together to form a three-dimensional matrix to generate $I \times J \times M$ multi-dimensional image. For ease of processing, a 3-D multi-dimensional image was converted into a $2-$D multi-dimensional image of $I \cdot J \times M$.

We set an image region, R, to contain N Pixels. Then, M registered images of the region were superimposed to form a multivariate image of region R. The pixels of region R were expanded in a fixed order to generate an $N \times M$ $2-$D matrixed multivariate image. Each variable of a multivariate image described the same pixel point and contained information that was relevant. The PCA [42] was conducted to process considerable relevant data, and the main information and features of multi-dimensional images were obtained through the PCA. For the M images of region R, the pixels were expanded in a fixed order to form M N$-$ dimensional image vectors $x_i\,(i = 1, 2, \ldots, M)\,, x_i = [x_{1i}, x_{2i} \ldots, x_{Ni}]^T$. The multivariate image X had $X = [x_1, x_2 \ldots, x_M]$.

In this paper, using PCA to analyze multivariate images, we can get the following formula:

$$\begin{aligned} E &= X - \sum_{a=1}^{A} t_a p_a^T \\ &= X - \sum_{a=1}^{A} p_a p_a^T \\ &= X(I - \sum_{a=1}^{A} p_a p_a^T) \end{aligned} \tag{10}$$

In the above formula, E represents the error matrix obtained by PCA, X represents the original multivariate image, A represents the A principal components of PCA analysis, p_a represents the principal component load vector, I represents the identity matrix, and p_a^T represents the transposition of the p_a matrix.

In this study, several qualified sample images and tested sample images were stacked to build a multivariate image.

Some elements of the kernel matrix $X^T X$ could be calculated in advance, reducing the computation of on-line detection and satisfying the real-time requirement of the detection system.

From the tested apple images, P independent intact samples of apple images were selected manually. The $I_{si}\,(i = 1, \ldots P)$ served as a standard to form the apple image. The tested image of the apple image to be examined was I_t. To verify whether there were surface defects in apple image. I_t, the standard apple image, I_{si}, and the tested apple image, I_t, were stacked to form multiple tested apple images with $P + 1$ variables. The image here was expanded to the N−dimensional vector $X_{si} = [X_{si1}, X_{si2}, \ldots, X_{siN}]^T$ and $X_{st} = [X_{st1}, X_{st2}, \ldots, X_{stN}]^T$. Then, a P + 1 multiple apple image X was built as $X = [X_{s1}, X_{s2}, \ldots, X_{sP}, X_t]$.

By performing a PCA, the load vector p_a of a principal component and the score vector T_a of a principal component were yielded for multivariate image X. Surface defects and other information in the apple image could be obtained from the obtained principal component score vector, T_a. By removing the first principal component (most variance information of the original image) and the last principal component (image noise), we formed the error matrix $E = X(I - (p_{first}p_{first}^T + p_{last}p_{last}^T))$.

2) EXTRACTION OF APPLE DEFECTS BASED ON Q-STATISTIC GRAPH

By processing the multivariate image data, we obtained the score vector image, T^a, and the simplified error matrix, E. Thus, different statistical information could be obtained to lay the basis for surface defect extraction.

Using the error matrix E to calculate Q statistics, E was written in the form of N-row vectors as follows:

$$E = [e_1^T, e_2^T, \ldots, e_N^T]^T \tag{11}$$

where $e_i\,(i = 1, \ldots, N)$ denotes the M-dimensional vector corresponding to the i-th pixel, and $e_i = [e_{i1}, e_{i2}, \ldots, e_{iM}]^T$. The Q-statistic of multivariable image Q was an N-dimensional vector, which was computed as follows:

$$q = [e_1^T e_1, e_2^T e_2, \ldots, e_N^T e_N]^T. \tag{12}$$

We expanded the order of pixels in accordance with area R. The Q-statistical image of the R region could be restored from the Q-statistic vector, Q. The Q-statistical image clearly reflected the image characteristics of the multivariate image during the test. Surface defect detection was then performed based on the Q statistic image to identify apple image features. In the Q statistic image, the defects of the surface were easy to extract using the threshold method. The threshold value could be obtained using the test statistics of multiple random intact apple samples. A multivariate image surface detection was then performed on multiple intact apple samples to generate their Q-statistical images. If the Q statistics of these good apple samples were less than a certain upper limit value, α, α would serve as the threshold of defect detection.

3) APPLE DEFECT DETECTION BASED ON MULTIVARIATE IMAGE ANALYSIS STRATEGY

In this paper, the Q statistic is used to detect the apple defect. Firstly, the maximum value α of the Q statistic is calculated according to the Q chart, and then α is used as the threshold for defect detection. When the apple defect is detected, the Q chart of the test image is subjected to binary processing and morphological filtering, and the point exceeding the threshold is detected as a defect.

The data set consisted of 2000 apple images, of which 800 were defective apple images, and 1200 were intact apple images. Apple defect detection was performed using a multi-image strategy. The steps were as follows:

Step 1: Twelve-hundred normal apple images were extracted from the data set, and 180 images were randomly selected as the standard images to construct multivariate images.

Step 2: For each of the other normal fruit images, a multivariate test image of the normal fruit sample was constructed based on 180 standard images. The upper limit value alpha was estimated from the Q-statistic images of the normal fruit samples, and alpha served as the threshold of the apple surface defect detection.

Step 3: A multivariate image was generated based on each defect image, and 180 standard images and the Q-statistic image of the tested image, was yielded using the multivariate image processing method.

Step 4: The Q statistic of the test image was processed using a threshold alpha, and the points beyond the threshold were detected as surface defects of the apple.

D. SELECTION OF DEFECT INDICATORS

To facilitate a quantitative analysis on the accuracy of the partial categorization of apple defects, the experimental results mentioned above were analyzed using four different quantitative indicators, including similarity index, over-segmentation rate, under-segmentation rate, and JS value. Meanwhile, the Ground Truth was applied as the assessment index. The indicators were defined as follows:

$$S = 2\,|A_i \cap B_i|\,/(|A_i| + |B_i|), \tag{13}$$

$$FPVF = (|B_i| - |A_i \cap B_i|)/\,|A_i|\,, \tag{14}$$

$$FNVF = = (|A_i| - |A_i \cap B_i|)/\,|A_i|\,, \tag{15}$$

$$JS\,(A_i, B_i) = (|A_i \cap B_i|)/(|A_i \cup B_i|). \tag{16}$$

In the Equation, A_i and B_i denote Ground Truth to delineate the apple's defect region and the apple's defect region separated by algorithm, respectively. The symbol $|*|$ represents the number of pixels contained within the region. S represents the similarity index, FPVF represents the over-segmentation rate, FNVF represents the under-segmentation rate, and JS represents the Jaccard's similarity index. Generically, a larger S value resulted in smaller $FPVF$ and $FNVF$ values, with the JS value increasingly approaching 1. This indicated that a higher accuracy in segmentation could be derived from

TABLE 2. Comparison of segmentation indexes between two methods.

Algorithm	S	FPVF	FNVF	JS
FCM-NPGA	97.08	3.06	3.23	93.52
FCM	90.12	3.56	15.02	81.72

Note: S: similarity index
FPVF: over-segmentation rate
FNVF: under-segmentation rate
JS: Jaccard's similarity index

segmentation results that were closer to the standard segmentation results.

III. ANALYSIS OF EXPERIMENTAL RESULTS

A. APPLE DEFECT SEGMENTATION BASED ON FCM-DPGA AND STANDARD FCM

After the low-level processing of the apple image with defects, the key problem was to detect the defective areas. The main question and the key to success in the whole defect detection process was whether the surface defect areas could be accurately segmented from the image.

In this paper, the genetic algorithm population is set to 30, and the number of iterations is 300 to approach convergence; the cross probability of 0.6 is used to accelerate convergence. Due to the strong randomness caused by mutation, in order to ensure that excellent individuals can achieve stable convergence at the same time, the mutation probability is set to 0.01.

In this study, the FCM-DPGA algorithm and the standard FCM algorithm were compared to observe the effect of apple segmentation, as shown in Fig. 8.

Fig. 8 (a)–(d) are based on the FCM-NPGA apple image segmentation graph. From Fig. 8 (a)–(d), the segmentation effect was highly consistent with the defective part of the original picture, which showed good connectivity. As shown in Fig. 8 (c), the apple cracks could be separated well, even when the apple surface defects were not obvious Fig. 8 (e) to 8 (h) are image defect segmentation images of the apple based on the standard FCM algorithm. Based on the results of the experimental simulation, we discovered that there was an obvious over-segmentation phenomenon in Fig. 8 (e)–(h). As the spatial relation information between image pixels was not used effectively in the segmentation of the standard FCM method, the segmented regions may not have been continuous. Because of the possibility of over-segmentation, the number of clusters in segmentation may not have been correct, and the segmentation result was different. When the image was more complex, and the segmentation effect was less than ideal, there were certain defects.

To further verify the superiority of FCM-NPGA segmentation, we conducted a statistical analysis of FCM-NPGA and the standard FCM methods. We set the identical number of iterations in the lab to 300. Fig. 9 shows the experimental results of three groups of image segmentation

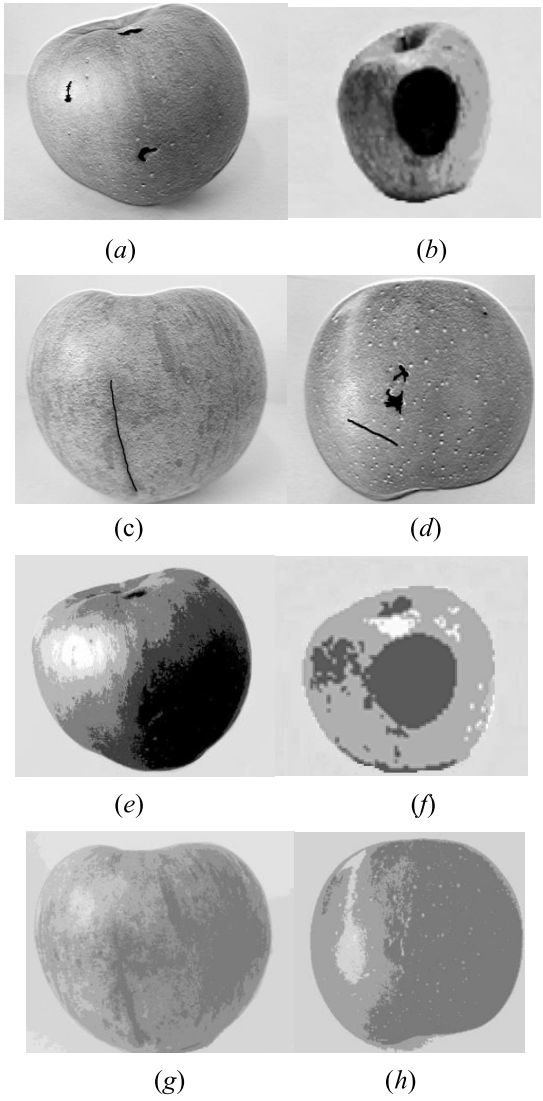

FIGURE 8. Apple defect segmentation between the FCM-NPGA and standard FCM algorithms. (a)-(d) are based on the FCM-NPGA apple image segmentation graph, (e) to (h) are image defect segmentation images of the apple based on the standard FCM algorithm.

techniques based on the FCM-NPGA and standard FCM image segmentation technology. The standard FCM was used as the basis for the control group. In accordance with the above experimental results, we carried out a numerical analysis. To increase the visualization of the data, the numerical analysis results were intuitively expressed in a histogram. Fig. 9 shows the comparison of the global consistency error value, the probability edge index, and the information change value of the two schemes.

As shown in Fig. 9, the segmentation method based on the FCM-NPGA basically minimized the *GCE* data. Compared with FCM, the data had obvious differences and were superior to the segmentation results of the standard FCM algorithm. The similarity between the experimental segmentation results and the marked standard images in the database was measured, and the *PRI* was obtained using a theoretical analysis with statistical mathematics. The *PRI* value of the algorithm

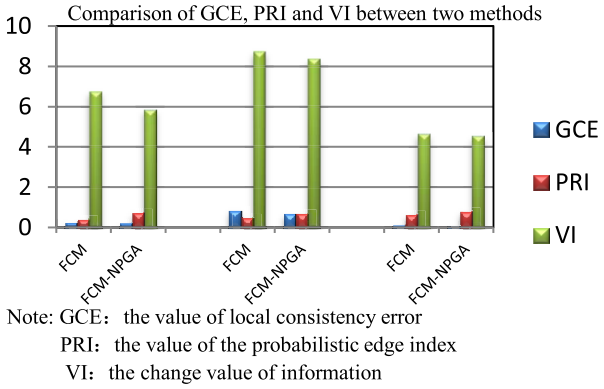

FIGURE 9. Comparison of GCE, PRI, and VI for FCM and FCM-NPGA.

used in this study was basically higher than that of the standard FCM algorithm. This indicated that the segmentation effect of this algorithm is better. *VI* refers to the size of the information transformation between a reference image and a segmented image. The *VI* value of the FCM-NPGA algorithm verified in this study was lower than that of the other methods. The segmentation method based on the FCM-NPGA tested in this study was compared with the standard FCM method, and the results showed that the FCM-NPGA had better similarity with the original image.

B. APPLE DEFECT DETECTION AND ANALYSIS BASED ON THE FCM-NPGA AND STANDARD FCM ALGORITHMS

In this study, apple defects were simultaneously detected using a multivariate image analysis method. The detection of segmented apple defect images was based on the FCM-FPGA algorithm, whereas that of the segmented apple defect map was based on the standard FCM algorithm. The effect of the two algorithms on the detection of defects in a multivariate image analysis was also observed.

The results of partial defect detection of an apple using the FCM-NPGA based segmentation algorithm are shown in Fig. 10, (*a*) to (*d*). Because of the complexity of the fruit defect image, there had to be a better Q-statistic chart of the test image. According to the adjustment of numerous experiments, $\alpha = 32$ was set. The results revealed that the FCM-NPGA-based segmentation algorithm could detect the apple defect region accurately and effectively.

The apple's partial defect detection results using the conventional standard FCM segmentation algorithm are shown in Fig. 10, (*e*) to (*h*). The detection failed to accurately mark out the apple defects, and were also affected by the fruit light and the shadow produced by clustering, including the non-defective parts of the fruit.

In order to make the analysis of the advantages of the detection algorithm simpler and more intuitive, a ROC curve was applied to assist with the assessment of the detection performance to be delivered by the detection algorithm. The apple defect image processed using this method was recorded as $A_{i,j}$, and Ground Truth was labeled as $B_{i,j}$. Equations (17) and (18) indicate how sensitivity S_n and specificity S_p were

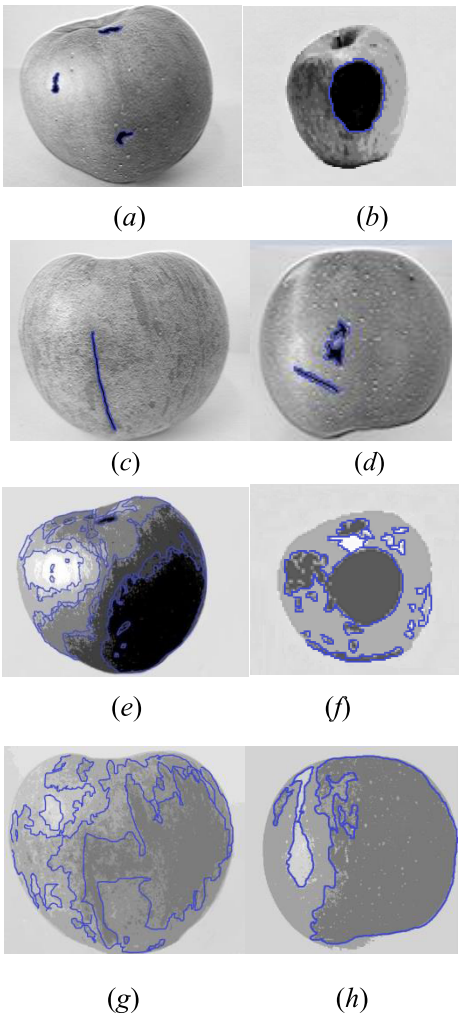

FIGURE 10. Apple defect detection based on FCM-NPGA and standard FCM algorithms. The results of partial defect detection of an apple using the FCM-NPGA based segmentation algorithm are shown in (a) to (d). The apple's partial defect detection results using the conventional standard FCM segmentation algorithm are shown in (e) to (h).

calculated, respectively.

$$S_n = \frac{1}{M}\sum_{i,j} A_{i,j} \bigcap B_{i,j} \tag{17}$$

$$\left(1 - S_p\right) = \frac{1}{N}\sum_{i,j} (1 - A_{i,j}) \bigcap B_{i,j} \tag{18}$$

where M represents the number of defective pixels contained in image $A_{i,j}$, N denotes the number of non-defective pixels contained in image $A_{i,j}$, and "$\bigcap$" signifies the intersection operation. The method was subjected to comparison to the defect detection results in accordance with standard FCM. Fig. 11 depicts the ROC curve.

As the figure above shows, the ROC curve of this method was found to approach the upper left corner most. We also spotted that the True Positive Rate was comparatively higher and had a lower False Positive Rate. This signaled that the detection method proposed in this study was more effective in detecting the defective parts of apples. The two algorithms

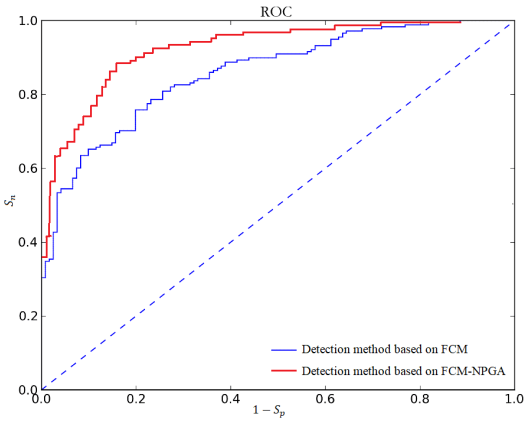

FIGURE 11. ROC curves for both methods.

TABLE 3. Comparison of runtime between two algorithms.

Algorithm	Number	Runtime
Detection algorithm based on FCM-NPGA	1000	22 min
Detection algorithm based on FCM	1000	42 min

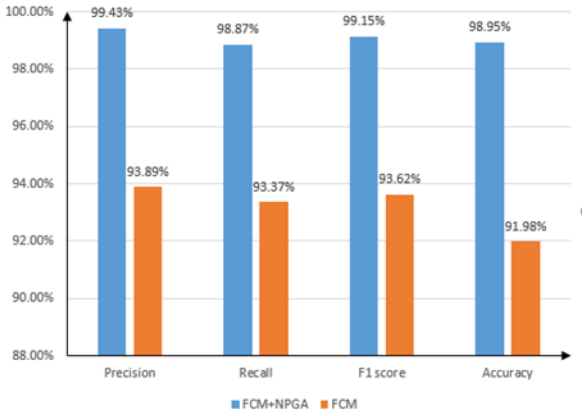

FIGURE 12. Evaluation indexes for both methods.

were compared for their respective runtimes, with the comparative results presented in Table 3.

From the comparison of the detection results, it can be seen that the Precision, Recall, F1-score, and Accuracy of defect detection based on the standard FCM image segmentation method are low. This was because there was a defect-uneven region in the apple image detected in the experiment, which exerted a great influence on the result of defect segmentation. The FCM-CPGA we proposed extracted the segmented image and carried on the local search to guarantee its global optimal solution, which helped obtain a better flaw segmentation result. As a result, the success rate of defect detection based on the FCM-NPGA image segmentation method was greatly increased. The experimental results in Table 2 and 3 show that the surface defect detection algorithm based on FCM-NPGA effectively improved the accuracy of apple defect detection and reduced the rate of missing detection. Thus, the reliability of the algorithm was high, and the detection effect was satisfactory.

IV. CONCLUSION

With the rapid development of computer vision, the image segmentation component has been processed by several algorithms. An algorithm for processing image segmentation is also undergoing optimization. In recent years, the GA has become the focus of scholars locally and abroad. In this study, the FCM and NPGA algorithms were combined into the FCM-NPGA, which treated the objective function of the FCM algorithm as the fitness function of GA. At the same time, in order to improve the local search ability, the detailed information of the geometric feature image itself was preserved. Based on the strong local search ability of nonlinear programming, the FCM-NPGA was proposed and implemented. The experimental results showed that this method performed well in geometric feature image segmentation, and combined with the multivariate image analysis method, the overall detection accuracy of apple skin defects reached 98%.

Existing research on GA has been very extensive and mature. In this study, a NPGA was proposed to obtain better results in object optimization image segmentation. Therefore, we should further explore the application of genetic theory in all kinds of fruit image segmentation, such as in image preprocessing in the early steps of segmentation. In this study, the preprocessing of apple image denoising and enhancement based on fractional calculus algorithm was applied, and good results were obtained. The results suggested that image preprocessing is a very important component of image segmentation. Therefore, in order to obtain good segmentation results, future work should aim at various categories of different features of the image research and analysis of preprocessing methods to adapt to their characteristics. At present, the objective evaluation indexes of images are mainly supervised evaluation methods. Although more accurate and reliable results can be obtained, there must be a manually marked standard image as a comparison in the process of evaluation. In addition to specialized experimental data, it is usually difficult, and sometimes impossible, to obtain standard images. Moreover, the evaluation index of unsupervised image segmentation has thus far been a low-level, data-driven evaluation method based on image features. The results of the evaluation, moreover, are often inaccurate. For the work of image segmentation, it is also necessary to establish a reasonable and accurate image segmentation evaluation system.

REFERENCES

[1] L. Ma, S. Bi, and C. Zhang, "Apple grading system based on near infrared spectroscopy and evidential classification forest," in *Proc. Int. Conf. Adv. Mech. Syst. (ICAMechS)*, Aug. 2019, pp. 326–330, doi: 10.1109/ICAMechS.2019.8861601.

[2] N. M. Baneh, H. Navid, and J. Kafashan, "Mechatronic components in apple sorting machines with computer vision," *Food Measure*, vol. 12, no. 2, pp. 1135–1155, Jun. 2018, doi: 10.1007/s11694-018-9728-1.

[3] Y. Tao and Z. Wen, "An adaptive image transform for high-speed fruit defect detection," *Trans. ASAE*, vol. 42, no. 1, pp. 241–246, Oct. 2013, doi: 10.13031/2013.13201.
[4] K. G. Dhal, A. Das, S. Ray, J. Gálvez, and S. Das, "Nature-inspired optimization algorithms and their application in multi-thresholding image segmentation," *Arch Comput. Methods Eng*, Mar. 2019, pp. 1–34, doi: 10.1007/s11831-019-09334-y.
[5] Q. Yang, "An approach to apple surface feature detection by machine vision," *Comput. Electron. Agricult.*, vol. 11, nos. 2–3, pp. 249–264, Nov. 1994, doi: 10.1016/0168-1699(94)90012-4.
[6] Y. Lu, Y. Huang, and R. Lu, "Innovative hyperspectral imaging-based techniques for quality evaluation of fruits and vegetables: A review," *Appl. Sci.*, vol. 7, no. 2, p. 189, Feb. 2017, doi: 10.3390/app7020189.
[7] Q. Lü and M. J. Tang, "Detection of hidden bruise on kiwi fruit using hyperspectral imaging and parallelepiped classification," *Procedia Environ. Sci.*, vol. 12, pp. 1172–1179, Jan. 2012, doi: 10.1016/j.proenv.2012.01.404.
[8] S. Zhang, X. Wu, S. Zhang, Q. Cheng, and Z. Tan, "An effective method to inspect and classify the bruising degree of apples based on the optical properties," *Postharvest Biol. Technol.*, vol. 127, pp. 44–52, May 2017, doi: 10.1016/j.postharvbio.2016.12.008.
[9] D. Elien, V. D. Mattias, and K. Janos, "Assessment of bruise volumes in apples using X-ray computed tomography," *Postharvest Biol. Technol.*, vol. 128, pp. 24–32, Jun. 2017, doi: 10.1016/j.postharvbio.2017.01.013.
[10] J. C. Keresztes, M. Goodarzi, and W. Saeys, "Real-time pixel based early apple bruise detection using short wave infrared hyperspectral imaging in combination with calibration and glare correction techniques," *Food Control*, vol. 66, no. 1, pp. 215–226, Aug. 2016, doi: 10.1016/j.foodcont.2016.02.007.
[11] P. Baranowski, W. Mazurek, and B. Witkowska-Walczak, "Detection of early apple bruises using pulsed-phase thermography," *Postharvest Biol. Technol.*, vol. 53, no. 3, pp. 91–100, Sep. 2009, doi: 10.1016/j.postharvbio.2009.04.006.
[12] B. Zhang, W. Huang, L. Gong, J. Li, C. Zhao, C. Liu, and D. Huang, "Computer vision detection of defective apples using automatic lightness correction and weighted RVM classifier," *J. Food Eng.*, vol. 146, pp. 143–151, Feb. 2015, doi: 10.1016/j.jfoodeng.2014.08.024.
[13] S. Q. Zhou, Y. B. Ying, and D. S. Shang, "Morphology based noninvasive detection for fragrant pears browning with magnetic resonance imaging," *J. Zhejiang Univ. (Eng. Sci.)*, vol. 46, no. 12, pp. 2141–2145, Dec. 2012, doi: 10.3785/j.issn.1008-973X.2012.12.002.
[14] Y. Tian, E. Li, L. Yang, and Z. Liang, "An image processing method for green apple lesion detection in natural environment based on GA-BPNN and SVM," in *Proc. IEEE Int. Conf. Mechatronics Autom. (ICMA)*, Aug. 2018, pp. 1210–1215, doi: 10.1109/ICMA.2018.8484624.
[15] M. Nie, Q. Zhao, Y. Xu, and T. Shen, "Machine vision-based apple external quality grading," in *Proc. Chin. Control Decis. Conf. (CCDC)*, Jun. 2019, pp. 5961–5966, doi: 10.1109/CCDC.2019.8832996.
[16] S. Singh and N. P. Singh, "Machine learning-based classification of good and rotten apple," *Recent Trends Commun., Comput., Electron.* Singapore: Springer, 2019, pp. 377–386, doi: 10.1007/978-981-13-2685-1_36.
[17] Y. Ji, Q. Zhao, S. Bi, and T. Shen, "Apple grading method based on features of color and defect," in *Proc. 37th Chin. Control Conf. (CCC)*, Wuhan, China, Jul. 2018, pp. 5364–5368, doi: 10.23919/chicc.2018.8483825.
[18] H. B. Song, C. D. Zhang, and J. P. Pan, "Segmentation and reconstruction of overlappedapple images based on convex hull," *Trans. Chin. Soc. Agricult. Eng.*, vol. 29, no. 3, pp. 163–168, Mar. 2013, doi: 10.3969/j.issn.10026819.2013.03.022.
[19] W. M. Zhao, C. Y. Ji, and Y. Y. Li, "Recognition of ripe apples images in natural growth conditions," *Sci. Technol. Eng.*, vol. 12, no. 27, pp. 6889–6891, Sep. 2012, doi: 10.3969/j.issn.1671-1815.2012.27.007.
[20] K. Chen, X. Zou, and J. Xiong, "Improved fruit fuzzy clustering image segmentation algorithm based on visual saliency," *Nongye Gongcheng Xuebao/Trans. Chin. Soc. Agricult. Eng.*, vol. 29, no. 6, pp. 157–165, Jun. 2013, doi: 10.3969/j.issn.1002-6819.2013.06.020.
[21] Y. J. Yang and L. Tu, "Fruit image segmentation based on ant colony algorithm," *Jiangsu Agricult. Sciences*, vol. 42, no. 9, pp. 382–3380, Jun. 2014, doi: 10.15889/j.issn.1002-1302.2014.09.287.
[22] L. F. Luo, X. J. Zou, and Y. Zhou, "Grape image fast segmentation based on improved artificial bee colony and fuzzy clustering," *Trans. Chin. Soc. Agricult. Machinery*, vol. 46, no. 3, pp. 23–28, Mar. 2015, doi: 10.6041/j.issn.1000-1298.2015.03.004.
[23] J. M. Prats-Montalbán and A. Ferrer, "Statistical process control based on Multivariate Image Analysis: A new proposal for monitoring and defect detection," *Comput. Chem. Eng.*, vol. 71, pp. 501–511, Dec. 2014, doi: 10.1016/j.compchemeng.2014.09.014.
[24] Z. Wang, "Application of GL fractional differential theory in remote sensing image enhancement," *Inf. Commun.*, vol. 1, no. 1, pp. 13–14, 2018, doi: 10.3969/j.issn.16731131.2018.01.005.
[25] R. Almeida, D. Tavares, and D. F. M. Torres, "Fractional calculus," in *The Variable-Order Fractional Calculus Variations*. Cham, Switzerland: Springer, 2019, pp. 1–19, doi: 10.5617/jeb.225.
[26] A. Carpinteri, P. Cornetti, and A. Sapora, "Nonlocal elasticity: An approach based on fractional calculus," *Meccanica*, vol. 49, no. 11, pp. 2551–2569, Nov. 2014, doi: 10.1007/s11012-014-0044-5.
[27] T. Odzijewicz, A. B. Malinowska, and D. F. M. Torres, "Fractional calculus of variations," *Balkan J. Geometry Its Appl.*, vol. 16, no. 2, pp. 523–537, Feb. 2015, doi: 10.1007/978-3-0348-0516-2_16.
[28] Y. Yang and Z. Zhou, "Research and implementation of image enhancement algorithm based on local mean and standard deviation," in *Proc. IEEE Symp. Electr. Electron. Eng. (EEESYM)*, Jun. 2012, pp. 375–378, doi: 10.1109/EEESym.2012.6258668.
[29] T. Rathi, R. P. Maheshwari, and M. Tripathy, "PSNR and robustness comparison between DCT and SVD based digital image watermarking against different noise and attacks," in *Proc. Int. Conf. Adv. Sci. Technol.* Cham, Switzerland: Springer, 2018, pp. 315–321, doi: 10.1007/978-3-030-15357-1_26.
[30] U. Sara, M. Akter, and M. S. Uddin, "Image quality assessment through FSIM, SSIM, MSE and PSNR-A comparative study," *J. Comput. Commun.*, vol. 7, no. vol. 3, pp. 8–18. 2019, doi: 10.4236/jcc.2019.73002.
[31] S. Shekar, C.-C. Chien, A. Hartel, P. Ong, O. B. Clarke, A. Marks, M. Drndic, and K. L. Shepard, "Wavelet Denoising of High-Bandwidth Nanopore and Ion-Channel Signals," *Nano Lett.*, vol. 19, no. 2, pp. 1090–1097, Feb. 2019, doi: 10.1021/acs.nanolett.8b04388.
[32] C. J. J. Sheela and G. Suganthi, "An efficient denoising of impulse noise from MRI using adaptive switching modified decision based unsymmetric trimmed median filter," *Biomed. Signal Process. Control*, vol. 55, Jan. 2020, Art. no. 101657, doi: 10.1016/j.bspc.2019.101657.
[33] J. Nayak, B. Naik, and H. S. Behera, "Fuzzy C-means (FCM) clustering algorithm: A decade review from 2000 to 2014," in *Proc. ICCIDM*, HI, USA, 2015, pp. 133–149, doi: 10.1007/978-81-322-2208-8_14.
[34] F. Wang, J. Li, S. Liu, X. Zhao, D. Zhang, and Y. Tian, "An improved adaptive genetic algorithm for image segmentation and vision alignment used in microelectronic bonding," *IEEE/ASME Trans. Mechatronics*, vol. 19, no. 3, pp. 916–923, Jun. 2014, doi: 10.1109/TMECH.2013.2260555.
[35] P. Ghamisi and J. A. Benediktsson, "Feature selection based on hybridization of genetic algorithm and particle swarm optimization," *IEEE Geosci. Remote Sens. Lett.*, vol. 12, no. 2, pp. 309–313, Feb. 2015, doi: 10.1109/lgrs.2014.2337320.
[36] H. X. Zhu, F. L. Wang, and W. T. Zhang, "Improved evolutionary strategy genetic algorithm for nonlinear programming problems," in *Proc. ICIEM*, Changsha, China, 2013, pp. 993–1003, doi: 10.1007/978-3-642-38391-5_105.
[37] F. Boukouvala, R. Misener, and C. A. Floudas, "Global optimization advances in mixed-integer nonlinear programming, MINLP, and constrained derivative-free optimization, CDFO," *Eur. J. Oper. Res.*, vol. 252, no. 3, pp. 701–727, Aug. 2016, doi: 10.1016/j.ejor.2015.12.018.
[38] J. Xiao, J. Lu, and X. Li, "Davies Bouldin index based hierarchical initialization K-means," *Intell. Data Anal.*, vol. 21, no. 6, pp. 1327–1338, Nov. 2017, doi: 10.3233/IDA-163129.
[39] P. Jolly and S. Raman, "Analyzing surface defects in apples using Gabor features," in *Proc. 12th Int. Conf. Signal-Image Technol. Internet-Based Syst. (SITIS)*, 2016, pp. 178–185, doi: 10.1109/SITIS.2016.36.
[40] A. R. Martins, C. S. Dourado, M. Talhavini, A. Braz, and J. W. B. Braga, "Determination of chronological order of crossed lines of ballpoint pens by hyperspectral image in the visible region and multivariate analysis," *Forensic Sci. Int.*, vol. 296, pp. 91–100, Mar. 2019, doi: 10.1016/j.forsciint.2019.01.021.
[41] G. Snoussi, E. Hamdi, and Z. Lafhaj, "Multivariate analysis methods based methodology for rock microcracking characterization," *Geotech. Geol. Eng.*, vol. 32, no. 4, pp. 973–986, Aug. 2014, doi: 10.1007/s10706-014-9773-4.
[42] H. P. Deutsch and M. W. Beinker, "Principal component analysis," *Derivatives Internal Models*. Cham, Switzerland: Palgrave Macmillan, 2019, pp. 793–804, doi: 10.1007/978-3-030-22899-6_34.

WENZHUO ZHANG was born in 1996. He received the bachelor's degree from the Central South University of Forestry and Technology, where is currently pursuing the master's degree. His main research direction of postgraduate study is forest fire prevention and graphic image processing.

JUAN HU is currently pursuing the bachelor's degree with the Central South University of Forestry and Technology, China. Her research interest includes the application of computer technology in the field of agriculture and image processing.

GUOXIONG ZHOU received the B.Sc. degree from Hunan Agricultural University, in 2002, and the M.Sc. and Ph.D. degrees from Central South University, China, in 2006 and 2010, respectively. He is currently an Associate Professor with the Central South University of Forestry and Technology. His main research interests include forest fire prevention and robotics.

MINGFANG HE received the Ph.D. degree in control science and engineering from Central South University, China, in 2015. She is currently teaching with the Central South University of Forestry and Technology. Her main research interests include science and engineering, specifically artificial intelligence.